Film-Cooling Effectiveness on a Rotating Turbine Platform Using Pressure Sensitive Paint Technique

A. Suryanarayanan

B. Ozturk

M. T. Schobeiri

J. C. Han

Department of Mechanical Engineering,
Texas A&M University,
College Station, TX 77843-3123

Film-cooling effectiveness is measured on a rotating turbine blade platform for coolant injection through discrete holes using pressure sensitive paint technique. Most of the existing literatures provide information only for stationary endwalls. The effects of rotation on the platform film-cooling effectiveness are not well documented. Hence, the existing three-stage turbine research facility at the Turbomachinery and Flow Performance Laboratory, Texas A&M University was redesigned and installed to enable coolant gas injection on the first stage rotor platform. Two distinct coolant supply loops were incorporated into the rotor to facilitate separate feeds for upstream cooling using stator-rotor gap purge flow and downstream discrete-hole film cooling. As a continuation of the previously published work involving stator-rotor gap purge cooling, this study investigates film-cooling effectiveness on the first stage rotor platform due to coolant gas injection through nine discrete holes located downstream within the passage region. Film-cooling effectiveness is measured for turbine rotor frequencies of 2400 rpm, 2550 rpm, and 3000 rpm corresponding to rotation numbers of Ro = 0.18, 0.19, and 0.23, respectively. For each of the turbine rotational frequencies, film-cooling effectiveness is determined for average film-hole blowing ratios of $M_{holes} = 0.5$, 0.75, 1.0, 1.25, 1.5, and 2.0. To provide a complete picture of hub cooling under rotating conditions, simultaneous injection of coolant gas through upstream stator-rotor purge gap and downstream discrete film-hole is also studied. The combined tests are conducted for gap purge flow corresponding to coolant to mainstream mass flow ratio of MFR = 1% with three downstream film-hole blowing ratios of $M_{holes} = 0.75$, 1.0, and 1.25 for each of the three turbine speeds. The results for combined upstream stator-rotor gap purge flow and downstream discrete holes provide information about the optimum purge flow coolant mass, average coolant hole blowing ratios for each rotational speed, and coolant injection location along the passage to obtain efficient platform film cooling.
[DOI: 10.1115/1.3142860]

1 Introduction

The initial stages of the turbine are constantly exposed to high temperatures from gases exiting the combustion chamber. For a given aerodynamic efficiency, any increase in the turbine inlet temperature translates to an increase in the thermal efficiency and hence the overall system efficiency. In pursuit of higher thermal efficiencies, gas turbines are operated at first stage inlet temperatures around 1500°C resulting in excessive thermal stresses on the turbine components. Continuous operation under high turbine inlet temperatures enhances the possibility of thermal failure of the hot gas path components. Also, the uniform temperature profile of the gases exiting the present day combustors further exposes the rotor platform to higher temperatures requiring effective thermal protection.

Film cooling is an external cooling technique commonly used in conjunction with internal cooling to protect the turbine components from the mainstream hot gas. In film cooling, a portion of the coolant used for internal cooling is ejected through discrete holes or slots over the surface of the components that need thermal protection. The coolant thus ejected displaces the mainstream boundary layer creating a protective film on the surface of the exposed component. This isolates the hot mainstream gas from the metal surface and considerably decreases the magnitude of the temperatures the hot gas path components encounter. The location of the coolant holes, their geometry, and the quantity of the coolant gases are critical in providing proper coolant film protection.

The research turbine facility used for the current work is described in detail by Schobeiri et al. [1–3]. The research turbine has the flexibility and capability to deal with current aerodynamics, film-cooling, and heat transfer issues. The secondary flow and its impact on efficiency and performance of turbine components are described extensively by Lakshminarayana [4] and Schobeiri [5]. Denton [6] gave an overview of the effects of different flow mechanisms including the secondary flow on turbomachinery losses. The platform surface is characterized by a highly complex 3D flow due to the viscous nature of the mainstream hot gases. A detailed model of the different types of vortices generated and the nature of the secondary flow on the platform surface has been put forth by several people in the past (Langston [7], Goldstein and Spores [8], Takeishi et al. [9], Sieverding [10], Herzig et al. [11], and Wang et al. [12]). Every model in general acknowledges the existence of a saddle point in the region near the blade leading edge on the platform beyond which the flow separates to give rise to pressure and suction side (SS) vortices commonly referred to as the horse shoe vortex. The pressure side (PS) of the horse shoe vortex, under the influence of the differential pressures existing across the pressure and suction surface of the adjacent blades, migrates toward the suction side and either attaches or flows over

Contributed by the International Gas Turbine Institute of ASME for publication in the JOURNAL OF TURBOMACHINERY. Manuscript received June 20, 2007; final manuscript received March 3, 2009; published online April 26, 2010. Review conducted by David Wisler. Paper presented at the ASME Turbo Expo 2007: Land, Sea and Air (GT2007), Montreal, QC, Canada, May 14–17, 2007.

or under the suction side of the horse shoe vortex, depending on the driving parameters. This vortex is commonly referred to as the passage vortex and almost always is detrimental to attempts made at platform cooling as it tends to lift the coolant off the surface. Further, the existence of several other secondary flow vortices also makes providing uniform platform cooling a difficult task. All the above investigations were conducted on a cascade, and the influence of rotation on the endwall flows and the subsequent effects on the coolant flow has not been investigated. An up to date summary of the existing literature dealing with the endwall aerodynamics, film cooling, and heat transfer is also provided by Han et al. [13], Simon and Piggush [14], and Bogard and Thole [15].

Platform film-cooling effectiveness investigations have been predominantly performed using cascade vanes due to the inherent complexities in designing and instrumenting rotating systems. One of the earliest studies on platform film cooling was performed by Blair [16] using an upstream slot in a large scale turbine vane passage. Harasgama and Burton [17] conducted heat transfer and aerodynamic measurements in an annular cascade fit with vanes under representative engine flow conditions. Their results show that film cooling reduced the Nusselt numbers near the suction side by about 50%, suggesting that the coolant was convected toward the suction side by the passage secondary flows. Friedrichs et al. [18,19] detailed the aerodynamic aspects of platform film cooling and the effectiveness distributions using the ammonia and diazo technique. The tests were performed in a large scale low-speed turbine cascade with four rows of film-cooling holes along four axial stations on the platform. The presence of secondary flows was found to erode the coolant film near the surface necessitating a detailed investigation of the flow phenomenon in this region. The film-cooling traces were observed to be pushed toward the suction side especially near the leading edge of the blade similar to that observed by Harasgama and Burton [17]. They also concluded that platform film cooling can increase aerodynamic losses due to the mixing of the coolant with the mainstream.

A review of heat transfer and cooling on a turbine nozzle platform has been done by Chyu [20]. Zhang and Jaiswal [21] investigated film cooling in a turbine nozzle endwall with two different upstream coolant hole geometries using pressure sensitive paint (PSP). Effects of coolant mass flow on the effectiveness and distribution of coolant gas were studied. Lower coolant mass flow was found to be less effective in counteracting the effects of secondary flow in the endwall region and hence led to lower film-cooling effectiveness. Higher coolant-to-mainstream mass flow ratios gave a more uniform effectiveness distribution. Kost and Nicklas [22], Nicklas [23], and Kost and Mullaert [24] studied the effects of film cooling and heat transfer on the endwall of a linear cascade. The location of the upstream cooling slot with respect to the blade leading edge was found to determine the effectiveness of film cooling. Slots positioned near the saddle point tended to reinforce the horse shoe vortex, and the increased turbulence washed away the effects of the coolant fluid decreasing film effectiveness. For cooling the platforms upstream of the blade passage, slot ejection was found to be more useful than discrete holes. Film cooling through holes enhanced the heat transfer coefficients as compared with the no blowing cases.

Tests on film-cooling effectiveness on contoured platforms were performed by Oke et al. [25–27] in a linear, low speed cascade. Coolant was injected through single and double slots upstream of the blades. Film-cooling hole patterns on the platform with several holes along with slot injection were studied by Knost and Thole [28] in a low speed cascade with nozzle guide vanes. Patterns with film-cooling holes along iso-Mach lines were found to give much better film coverage. The effect of a back facing step before coolant injection was studied by Zhang and Moon [29] to simulate realistic engine geometry conditions. They used PSP to determine the film-cooling effectiveness and found that a back facing step caused an unstable boundary layer and damaged film coverage. Component misalignment with a forward as well as a backward step, at the upstream injection slot and on the slashface gap, was investigated by Piggush and Simon [30]. They studied flow and loss characteristics associated with these features and noticed that blowing through the slashface gap has the most significant impact on the passage losses. Similar assembly features were also studied by Cardwell et al. [31]. Hada and Thole [32] computationally predicted the film-cooling effectiveness with upstream and midpassage slots on turbine endwall and also for the height difference between the upstream slot and the downstream endwall. Adiabatic film-cooling effectiveness using wide banded thermochromic liquid crystals was measured on the turbine endwall nozzle vane cascade by Barigozzi et al. [33] for fan shaped holes with different area ratios. The secondary flow was suppressed for the smaller area ratios as the coolant exiting the holes had higher momentum to overcome the effects of the secondary flow, thus decreasing the secondary losses. As expected an increase in hole area ratio ensured wider spread for the exiting coolant.

Experimental studies available in open literature on film cooling and heat transfer on rotating turbine blades and their components are few and far between, primarily due to the difficulty in instrumenting rotating parts. Dring et al. [34] investigated film-cooling performance in a low speed rotating facility with a film-cooling hole that was positioned on both the pressure and suction sides of the blade. They used ammonia and Ozalid paper to qualitatively observe the coolant trace while the quantitative tests were conducted using thermocouples. Their results showed that the film coolant had only a small radial displacement, similar to flat plate results, on the suction side. On the pressure side, the film-coolant trace had a large radial displacement toward the blade tip. Effectiveness distributions on the blade span for a rotating turbine blade were also provided by Takeishi et al. [35] and Abhari and Epstein [36] using gas chromatography and thin-film heat flux gauges, respectively. Blair [37] studied the heat transfer on the pressure and suction sides as well as on the hub platform surface for a rotating turbine model. Enhanced heat transfer was observed on the platform due to the secondary flow effects. Recently, Ahn et al. [38,39] investigated the film-cooling effectiveness on the leading edge of a rotating blade for two row and three row coolant injections on the leading edge at design and off-design rotating conditions. Off-design conditions were found to significantly alter the film-coolant traces on the leading edge. The same experimental facility has been used in this paper with a new turbine rotor to allow for stator-rotor gap and downstream discrete-hole cooling.

The PSP technique for film-cooling effectiveness is based on mass transfer analogy and is free from heat conduction related errors frequently encountered with other heat transfer measurement techniques measuring adiabatic effectiveness. A complete map of local film-cooling effectiveness distribution on the rotor platform surface can be obtained rather than just a few discrete points obtained using heat flux gauges or thermocouples. The results from this technique have been calibrated with other measurement techniques by Wright et al. [40] on a film cooled flat plate, Gao et al. [41] on a film cooled turbine blade leading edge model, and Wright et al. [42] on a turbine cascade platform film-cooling study. A detailed working methodology of PSP to measure film-cooling effectiveness has been described by Wright et al. [40]. Since no heating is involved, errors arising from lateral heat conduction in the test surface are avoided, resulting in a distinct and well-defined coolant trace. The results from this technique have also been successfully demonstrated by Ahn et al. [43] and Mhetras et al. [44] on blade tip film cooling. Leading edge film-cooling effectiveness tests in a rotating frame using the PSP method have also been performed by Ahn et al. [38,39].

Suryanarayanan et al. [45] investigated the rotational effects on first stage rotor upstream gap ejected film-cooling effectiveness using PSP on the same test facility used for the current paper. Increasing the rotational speed from 1500 rpm to 2550 rpm increased the magnitude of local film-cooling effectiveness for up-

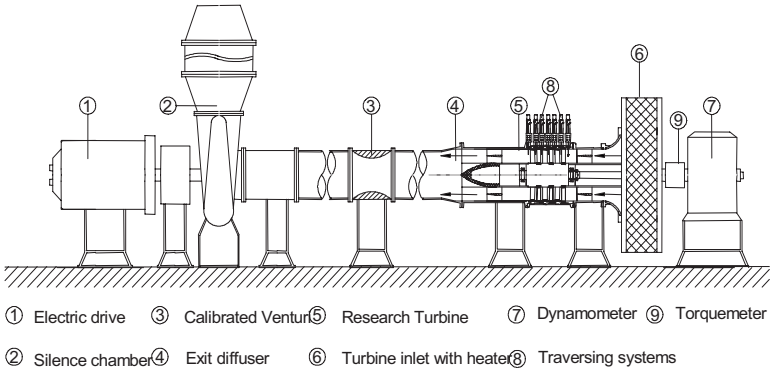

Fig. 1 The overall layout of TPFL-research turbine facility, from Schobeiri et al. [1–3]

stream stator-rotor gap injection. They also concluded that as the coolant to mass flow ratio of upstream injection was increased from 0.5% to 2.00%, the effectiveness magnitude and distribution on the platform surface increased. The coolant from the upstream slot affected by the inlet flow incidence and passage vortex tended to concentrate close to the blade suction side of the platform. The stator-rotor gap purge flow did not provide sufficient film protection on the downstream region and along the pressure surface on the rotor platform for the coolant to mass flow ratios tested. Hence, to shield the downstream region and understand the effects of rotation on downstream hole coolant injection, the present paper focuses on measuring film-cooling effectiveness on the first stage rotor platform of a three-stage research turbine using nine discrete film-cooling holes for three rotational speeds and several blowing ratios. In addition, film-cooling tests were also conducted with simultaneous upstream stator-rotor gap and downstream discrete-hole injection to understand the interaction between the methods of injection under rotation.

2 Experimental Facility

The gas turbine facility used for the current experiments was designed by Schobeiri [1] to address aerodynamic performance and heat transfer issues of high pressure (HP), intermediate pressure (IP), and low pressure (LP) turbine components. Detailed aerodynamic, efficiency, loss, and performance measurements were carried out to verify and document the efficiency and performance of a high-efficiency 3D, bowed blading in Ref. [1]. To compare the results of the investigations reported in Ref. [1] with those for 2D cylindrical blades, aerodynamic measurements were conducted and summarized in the subsequent reports [2,3]. To determine the film-cooling effectiveness under rotating conditions for leading edge film cooling [38,39], the existing turbine rotor described in Ref. [1] was modified to integrate the coolant loop through the downstream section of the hollow turbine shaft and into the cylindrical hub cavity. The facility had to be further modified to accommodate the coolant loops for platform discrete-hole film cooling and stator-rotor gap purge flow film cooling.

The overall layout of the test facility is shown in Fig. 1. It consists of a 300 hp electric motor connected to a frequency controller which drives a three-stage centrifugal compressor capable of supplying air with a maximum pressure difference of 55 kPa and a volumetric flow rate of 4 m^3/s. The compressor operates in suction mode and its pressure and volume flow rate can be varied by the frequency controller operating between 0 Hz and 66 Hz. A pipe with a smooth transition piece connects the compressor to a Venturi mass flow meter used to measure the mass flow through the turbine component. The three-stage turbine has an automated data acquisition system for detailed flow measurement at each blade row location in the radial and circumferential directions. The turbine inlet has an integrated heater that prevents condensation of water from humid air expanding through the turbine during experiments. The turbine shaft is connected, through a flexible coupling, to one end of a high precision torque meter that has a maximum rotational speed of 8500 rpm and a maximum torque rating of 677.9 N m. The other end of the torque meter is coupled via a second flexible coupling to an eddy current low inertia dynamometer with a maximum power capacity of 150 kW and a maximum torque of 500 N m.

3 New Turbine Component Design

A completely new three-stage turbine rotor component, as shown in Figs. 2 and 3, was designed with the dimensions and operating conditions specified in Table 1 to replace the one discussed in Refs. [1,3,38,39]. In addition to the tasks performed by

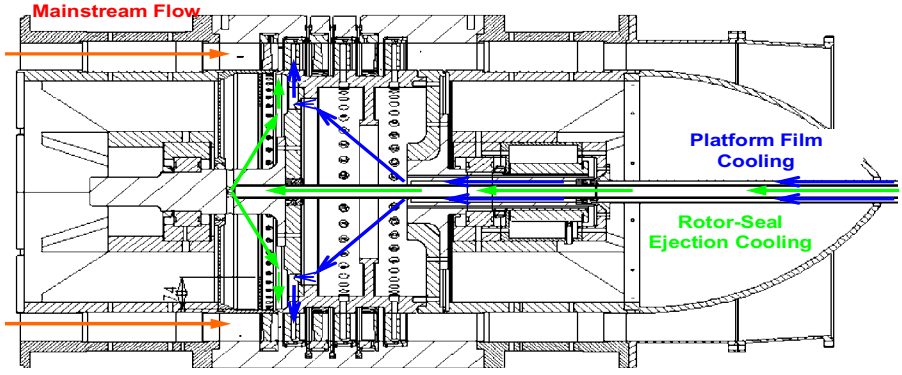

Fig. 2 Section view of the modified stator-rotor turbine assembly for stator-rotor purge flow and platform film cooling

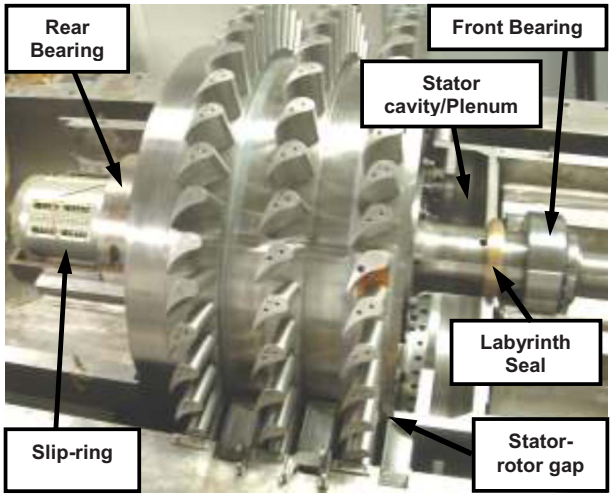

Fig. 3 Turbine rotor component with the 24-channel slip ring, stator cavity, and labyrinth seal

the old rotor, the new rotor was designed to operate at high speeds of 8500 rpm, close to the transonic range. The first critical speed for the new rotor occurs at 6500 rpm. Two independently controlled concentric coolant loops provide the necessary mass flow for all the platform film-cooling experiments. The outer loop supplies coolant for film-cooling experiments for the discrete film-cooling holes on the platform in the blade passage section. Nine discrete compound angled coolant holes of 1 mm diameter are machined on the first stage rotor platform as per the angles shown in Table 2. The holes are located about 50% downstream of the blade passageway. The approximate pitch to diameter ratio for the holes is 5 in the axial and tangential directions. The graphic representation of the coolant hole location on the platform is shown in Figs. 4 and 5. The inner loop supplies coolant mass for film-cooling experiments on the hub platform through upstream stator-rotor circumferential gap positioned between the first stage stator and rotor. A concentric jet exits this circumferential gap at an angle of 25 deg into the mainstream (Figs. 3–5). The maximum normal gap width is designed to be 3 mm. However, it can be decreased to up to 0.5 mm by translating the entire rotor toward the front bearing. For the current study it was set to 2.3 mm. The axial stator-rotor gap from the first stage rotor leading edge was measured at 5 mm. Similar to the optimization of the trailing edge slot ejection described in detail by Schobeiri [46] and Schobeiri and Pappu [47], the reduction in slot width is instrumental in establishing an optimum ejection ratio while keeping the cooling mass flow constant.

The blades attached to the new rotor were taken from the rotor described in Refs. [1,3,38,39]. They are typical HP-turbine blades used in steam turbines characterized by a relatively thick leading

Table 1 Turbine dimensions and operating conditions

Stage No., N	3
Mass flow	3.728 kg/s
D_t	685.8 mm
D_h	558.8 mm
Reference speed	2550 rpm
Speed range	2400–3000 rpm
Inlet pressure	101.356 kPa
Exit pressure	71.708 kPa
Power	80–110 kW
Blade height	63.5 mm
Blade No.	Stator 1=56
Blade No.	Rotor 1=46
Blade No.	Stator 2=52
Blade No.	Rotor 2=40
Blade No.	Stator 3=48
Blade No.	Rotor 3=44
α_2	19 deg
β_3	161 deg
α_3	110 deg
ϕ	0.353
λ	1.0
r	0.5

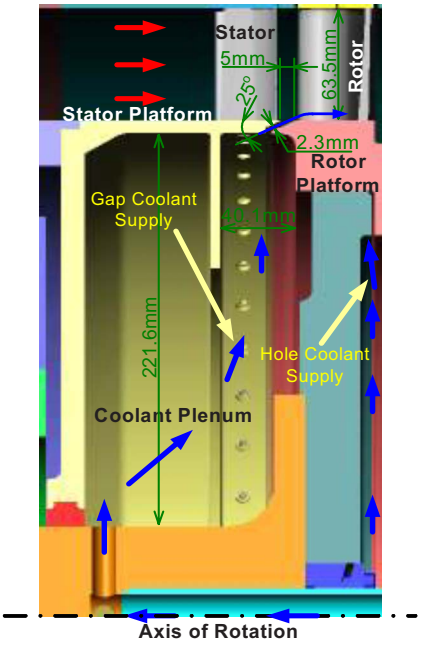

Fig. 4 Detailed view of the stator-rotor gap

Table 2 Film-cooling hole orientation

	D (mm)	γ (deg)	θ (deg)
Hole 1	1.00	35	47.39
Hole 2	1.00	35	34.50
Hole 3	1.00	35	25.31
Hole 4	1.00	35	49.58
Hole 5	1.00	35	42.29
Hole 6	1.00	35	32.62
Hole 7	1.00	37	57.46
Hole 8	1.00	37	40.25
Hole 9	1.00	37	33.83

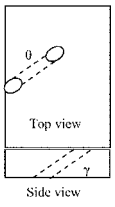

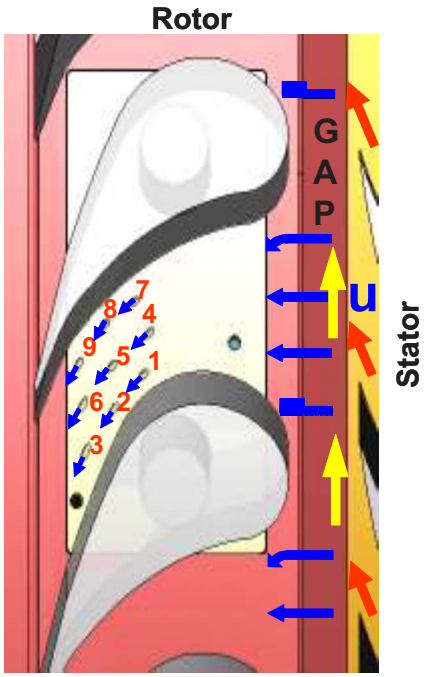

Fig. 5 Detailed view of rotor platform film-cooling holes

edge portion. This particular blade design allows reducing the total pressure losses due to the adverse off-design incidence changes caused by part-load operation. Thus, these blades are not characteristic of power generation or aircraft gas turbines. Although the blade geometry does not represent typical gas turbine blade geometry, it provides the basic features to extract information relevant to gas turbine design community. These features are (a) stator-rotor unsteady interaction, (b) blade and platform rotation and consequent exposure of the platform boundary layer to centrifugal and Coriolis forces, and (c) the flow acceleration. Except for the last feature (c), none of the above features can be simulated in a cascade investigation. To ensure that no coolant escapes through the rotary-stationary interfaces, the internal and external loops were sealed with labyrinths. The teeth spacing and the tip clearance were taken using the design instructions detailed by Schobeiri [5]. A 24-channel slip-ring is mounted to the rear shaft as shown in Fig. 3 to transfer temperature data from thermocouples from the rotating frame to the data acquisition system.

4 Film-Cooling Effectiveness Measurement Theory and Data Analysis

Data for film-cooling effectiveness are obtained using the PSP technique. PSP consists of photo luminescent molecules held together by a binding compound. The luminous particles in the PSP emit light when excited, with the emitted light intensity being inversely proportional to the partial pressure of oxygen in the surroundings. The emitted light intensity can be recorded using a charge coupled device (CCD) camera, and corresponding oxygen partial pressures can be obtained by calibrating emitted intensity against the partial pressure of oxygen. The image intensity obtained from PSP by the camera during data acquisition is normalized with a reference image intensity taken under no-flow conditions. Background noise in the optical setup is removed by subtracting the image intensities with the image intensity obtained under no-flow conditions without excitation. The resulting intensity ratio can be converted to pressure ratio using the previously determined calibration curve and can be expressed as

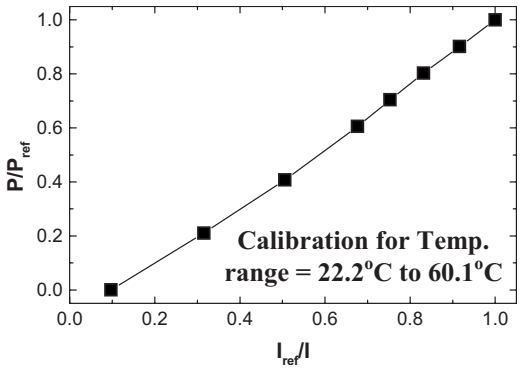

Fig. 6 Sample PSP calibration curve

$$\frac{I_{\text{ref}} - I_{\text{blk}}}{I - I_{\text{blk}}} = f\left(\frac{(P_{O_2})_{\text{air}}}{(P_{O_2})_{\text{ref}}}\right) = f(P_{\text{ratio}}) \tag{1}$$

where I denotes the intensity obtained for each pixel and $f(P_{\text{ratio}})$ is the relation between intensity ratio and pressure ratio obtained after calibrating the PSP. Further details in using PSP for pressure measurements are given by McLachlan and Bell [48].

Calibration for PSP was performed using a vacuum chamber at several known pressures varying from 0 atm to 1 atm with corresponding emitted intensity recorded for each pressure setting. The same optical setup is chosen for calibration as well as for data acquisition during the experiments to minimize any possible instrumentation errors. A sample calibration curve is shown in Fig. 6. PSP is sensitive to temperature with higher temperatures resulting in lower emitted light intensities. Hence, the paint was also calibrated for temperature. It was observed that if the emitted light intensity at a certain temperature was normalized with the reference image intensity taken at the same temperature, the temperature sensitivity can be eliminated. Hence, during data acquisition, the reference image was acquired immediately after the experiment was completed to avoid errors related to temperature variation. Reference images were acquired after the rotor came to a halt, and the temperature change from loaded to stationary condition was small enough to disregard its effect on PSP measurement. Coolant flow and platform surface temperatures were monitored using thermocouples placed along the individual coolant loops and on the platform surface close to the suction side, respectively. The thermocouples were wired through the slip-ring and connected to a microprocessor thermometer with a digital readout.

To obtain film-cooling effectiveness, air and nitrogen were used alternately as coolant. Nitrogen, which can be assumed to have the same molecular weight as that of air, displaces the oxygen molecules on the surface, causing a change in the emitted light intensity from PSP. By noting the difference in emitted light intensity and subsequently the partial pressures between the air and nitrogen injection cases, the film-cooling effectiveness can be determined using the following equation:

$$\eta = \frac{C_{\text{mix}} - C_{\text{air}}}{C_{N_2} - C_{\text{air}}} = \frac{C_{\text{air}} - C_{\text{mix}}}{C_{\text{air}}} = \frac{(P_{O_2})_{\text{air}} - (P_{O_2})_{\text{mix}}}{(P_{O_2})_{\text{air}}} \tag{2}$$

where C_{air}, C_{mix}, and C_{N_2} are the oxygen concentrations of mainstream air, air/nitrogen mixture, and nitrogen on the test surface, respectively, and are directly proportional to the partial pressure of oxygen.

The accuracy of the PSP technique for measuring film-cooling effectiveness has been compared by Wright et al. [40] on a flat plate with compound angled ejection holes against several measurement techniques such as steady and transient liquid crystal, infrared (IR) camera, and using a foil heater with thermocouples. Results were obtained for a range of blowing ratios and showed consistency with each other. Wright et al. [40] found that IR,

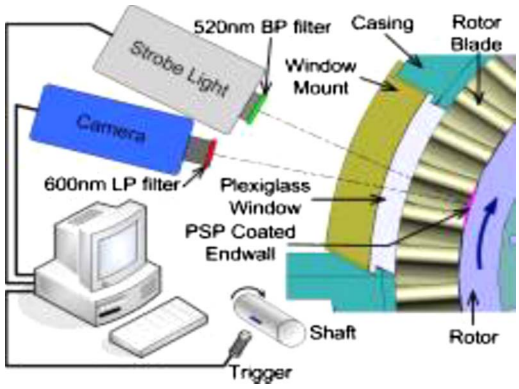

Fig. 7 Optical setup for PSP data acquisition

temperature sensitive paint (TSP), as well as PSP gave effectiveness results within 15% of each other. Larger uncertainties for heat transfer techniques such as IR and TSP methods were observed due to lateral conduction in the flat plate.

5 Experimental Procedure

The platform passage under investigation was layered with seven to nine coats of PSP using an air brush. This coated surface was excited using a strobe light fitted with a narrow bandpass interference filter with an optical wavelength of 520 nm. Upon excitation from this green light, the PSP coated surface emitted red light with a wavelength higher than 600 nm. A 12 bit scientific grade CCD camera (high speed SensiCam with CCD temperature maintained at $-15\,^{\circ}\mathrm{C}$ and using a two-stage Peltier cooler) fit with a 35 mm lens and a 600 nm longpass filter was used to record intensity images. The filters were chosen such that the camera blocked the light reflected from the target surface and only captured the actual data. A schematic of the optical setup used in the data acquisition is shown in Fig. 7. The camera, the strobe light, and the data acquisition system were triggered simultaneously using an optical sensor triggered off the rotor shaft. By detecting the same angular position, the camera was able to view the same region of interest at every rotation, making it possible to average the image intensities without blurring the information. A minimum exposure time of 17 μs was used for image capture from the camera. Estimated rotor movement during image capture at 2550 rpm for a 17 μs exposure time was approximately 1.1 mm. A total of 200 images were captured for each experiment with air and nitrogen injection, and the pixel intensity for all images was averaged. The image resolution obtained from the camera was 0.8 mm/pixel for a 4×4 binning on the camera. A computer program was used to convert these pixel intensities into pressure using the calibration curve and then into film-cooling effectiveness. The coolant flow rate was set using a rotameter based on prior calculation for the desired blowing and mass flow ratio. The coolant was heated to the same temperature as mainstream air ($45\,^{\circ}\mathrm{C}$) before injection through the gap to eliminate the temperature effects of PSP.

Uncertainty calculations were performed based on a confidence level of 95% and are based on the uncertainty analysis method of Coleman and Steele [49]. Lower effectiveness magnitudes have higher uncertainties. For an effectiveness magnitude of 0.8, uncertainty was around $\pm1\%$, while for an effectiveness magnitude of 0.07, uncertainty was as high as $\pm10.3\%$. This uncertainty is the cumulative result of uncertainties in calibration (4%) and image capture (1%). The absolute uncertainty for effectiveness varied from 0.01 to 0.02 units. Thus, relative uncertainties for very low effectiveness magnitudes can be very high ($>100\%$ at an effectiveness magnitude of 0.01). However, it must be noted that very few data points exist with such high relative uncertainty magnitudes. Uncertainties for the average blowing ratio calculations are estimated to be approximately 3.5% using Kline–McClintock analysis and discussed in detail by Holman [50].

6 Results and Discussion

This section presents the results obtained from the film-cooling experiments performed on the first stage rotor platform for downstream discrete-hole coolant injection. Experiments were conducted at three rotational speeds, 2400 rpm, 2550 rpm, and 3000 rpm, with the average film hole blowing ratios of $M_{\mathrm{holes}}=0.5$, 0.75, 1.00, 1.25, 1.50, 1.75, and 2.00. The Reynolds number based on the rotor axial chord length and the exit velocity was around 200,000 and the pressure ratio was 1.12 for the first stage. The rotation numbers corresponding to 3000 rpm, 2550 rpm, and 2400 rpm are 0.23, 0.19, and 0.18, respectively. Film-cooling effectiveness was calculated by applying the calibration curves to the intensity fluctuation captured by the camera between air and nitrogen injection. Overall it is found that film-cooling effectiveness is maximum as we approach an approximate average blowing ratio of $M_{\mathrm{holes}}=1.00$ for all three rotational speeds. The reference rotational speed of 2550 rpm has the maximum effectiveness among all rotational speeds for all blowing ratios. Platform cooling using simultaneous upstream slot and downstream discrete-hole injection yielded results similar to the individual blowing cases with little to no effects due to synchronized coolant ejection for MFR $=1\%$ and $M_{\mathrm{holes}}=0.75$, 1.00, and 1.25.

6.1 Reference Rotating Case. Film-cooling results on the effects of rotational speed performed by Ahn [38,39] showed that the location of the leading edge stagnation line, which yielded symmetric spreading of coolant on the suction and pressure surfaces of the leading edge, was at a rotational speed of 2550. This rotational speed was chosen as the reference rotating condition for the current investigation. Figure 8 shows film-cooling effectiveness on the rotor platform for downstream hole film cooling for the reference speed, 2550 rpm, and all the blowing ratios. As expected film-cooling effectiveness is maximum near the coolant hole exit. As we proceed downstream of the holes, effectiveness magnitude diminishes as the coolant mixes with the mainstream flow. Peak effectiveness values occur as we approach $M_{\mathrm{holes}}=1$ and are approximately equal to $\eta=0.70$ exactly where the coolant ejects out of the holes. Effectiveness values and film distribution begin to decrease below and above $M_{\mathrm{holes}}=0.75$ and 1.25, respectively. M_{holes} in this range provide good film-cooling protection on the platform covering most of the downstream passage surface. The contribution of each hole toward effective film coverage also varies depending on its location on the platform surface.

Since coolant density is assumed to be the same as that of the mainstream, M_{holes} is dependent only on the exit velocity of the coolant gas. For $M_{\mathrm{holes}}=1.00$, the velocity of the coolant ejecting out of the individual holes is approximately the same as that of the mainstream relative velocity at the first stage rotor exit. As the coolant flow velocity approaches the mainstream relative velocity, it appears that the ejected coolant has just the right momentum to adhere to the platform surface, displacing the mainstream boundary layer and minimizing the effects of the secondary flows. This allows the coolant to provide better film coverage and higher effectiveness magnitudes as minimal coolant is dissipated into the mainstream flow before providing any protection. At M_{holes} lower than 0.75, the coolant quantity for film cooling is small and is incapable of providing any effective protection on the platform surface. The lower momentum prevents the coolant from penetrating the boundary layer on the platform surface, hindering the development of an effective thermal barrier. The low momentum coolant tends to get carried away by the higher momentum mainstream flow decreasing the effectiveness. On the contrary, the ejected coolant for M_{holes} higher than 1.25 possesses larger momentum and has a tendency to lift-off as it leaves the coolant holes. The high velocity coolant merges with the mainstream im-

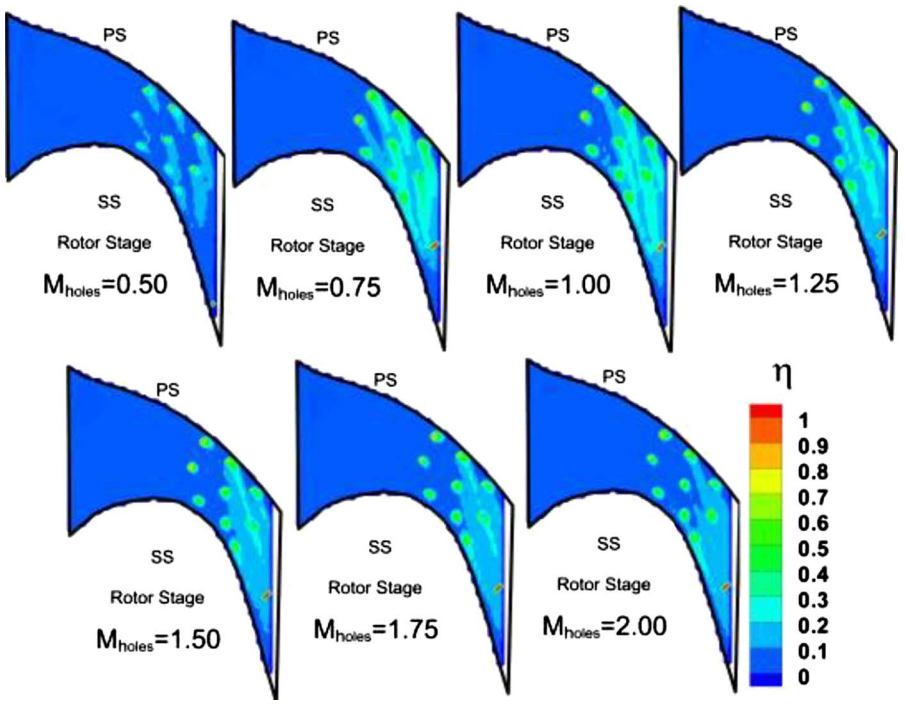

Fig. 8 Film-cooling effectiveness distribution on the film-cooling holes for all blowing ratios at 2550 rpm

mediately having little time to shield the platform surface. This effect of coolant mass on film effectiveness is similar to that seen by Zhang and Jaiswal [21] with their experiments on a linear cascade.

The coolant distribution on the platform is predominantly governed by the mainstream and secondary flow characteristics. The secondary flow generated by the pressure differential between neighboring blades influences the behavior of coolant gas in their path and significantly affects the capability of the coolant to offer uniform thermal protection. The coolant under the effects of the secondary flow is drawn toward the suction surface, leading to better protection near the suction surface. This movement of the coolant to the suction side under the influence of the platform secondary flow has also been documented by researchers [17,18,21] experimenting with cascades. The higher tangential velocity of the coolant jet under rotation also increases the migration of the coolant from the pressure side to the suction side on the platform. Interestingly, holes 1 and 4 (Fig. 5) show lower effectiveness and coolant coverage compared with the other holes. It is believed that these two holes lie in the path of the passage vortex and hence the coolant ejected through them is immediately dissipated into the mainstream. It can be deduced that providing protection closer to the suction surface is relatively easier due to the tendency of the coolant to flow toward the suction surface.

6.2 Effect of Rotation on Film Cooling. At rotational speeds lower than the reference speed, the blade flow deflection becomes larger, leading to higher specific stage load coefficient, and the stagnation region moves toward the pressure side as the flow incidence angle increases, as sketched in Fig. 9. Similarly, higher rotational speeds lead to negative incidence angle and cause the stagnation region to move toward the suction side. The pressure gradient on the platform across the pressure and suction side is affected by the change in the incidence angle based on the rotational speed change. This will alter the location of formation and the strength of the passage vortex and other secondary vortices that affect platform film cooling. Figures 10 and 11 show the film-cooling effectiveness distribution for off-reference rotational speeds of 2400 rpm and 3000 rpm. The figures contain contour plots for all the blowing ratios with the arrows depicting the geometric orientation of the coolant holes on the platform. Under no mainstream flow, the coolant exiting the holes is assumed to follow the arrow direction. Overall, it is seen that the effectiveness values for off-reference speeds are lower when compared with the reference speed. A reference speed of 2550 rpm has larger areas of

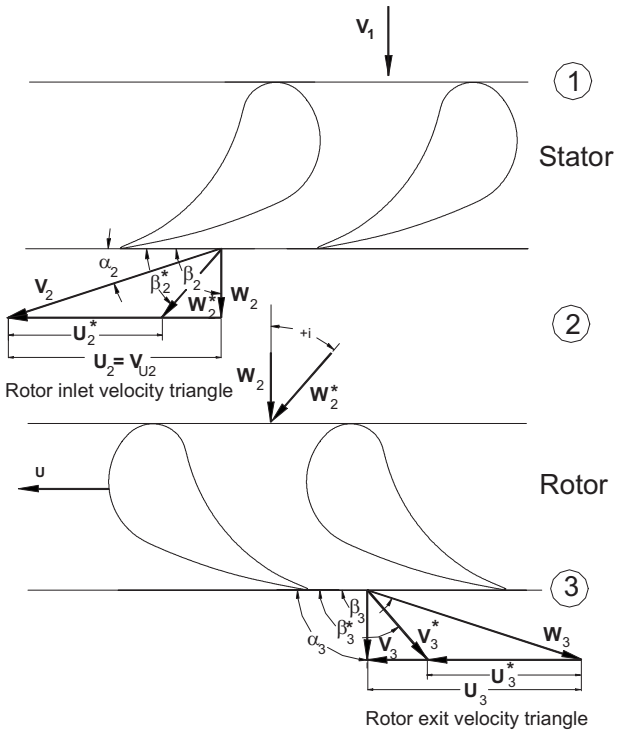

Fig. 9 Velocity triangles and relative inlet and exit flow angles design speed and for off-design rotating speeds

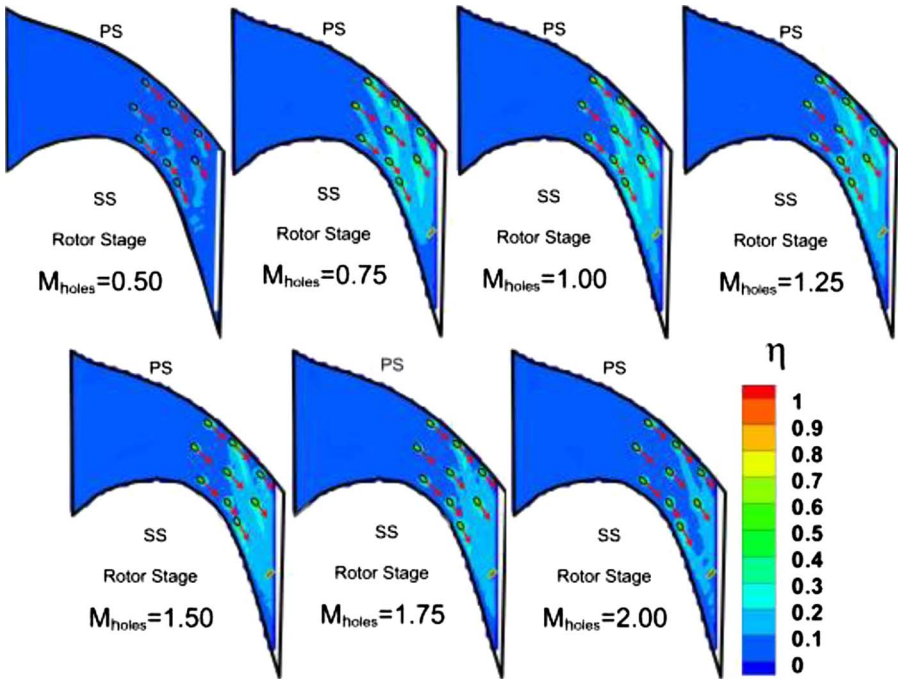

Fig. 10 Film-cooling effectiveness distribution on the film-cooling holes for all blowing ratios at 2400 rpm

the platform with higher film-cooling effectiveness though the peak effectiveness lies in the same range as the off-design speeds. Blowing ratios below 0.75 and above 1.25 provide minimal protection to the platform surface irrespective of the rotational speeds. The coolant traces once again follow the cross flow from the pressure side to the suction side.

Maximum effectiveness for 2400 rpm occurs between $M_{\text{holes}}=1.00$ and 1.25 and for 3000 rpm it is between $M_{\text{holes}}=0.75$ and 1.00. The effectiveness magnitudes for both cases show a peak value of approximately $\eta=0.70$ close to the coolant hole exit. Varying the rotational speed over or under the reference speed affects the coolant distribution on the platform surface with the higher rotational speed, showing the lowest coolant coverage. At rotational speeds lower than the reference speed and for the same blowing ratio, the coolant mass ejected through the holes is smaller and hence has a lower relative velocity than the reference case. Similarly at higher rotational speeds the coolant ejecting out of the holes has a higher relative velocity due to the higher coolant

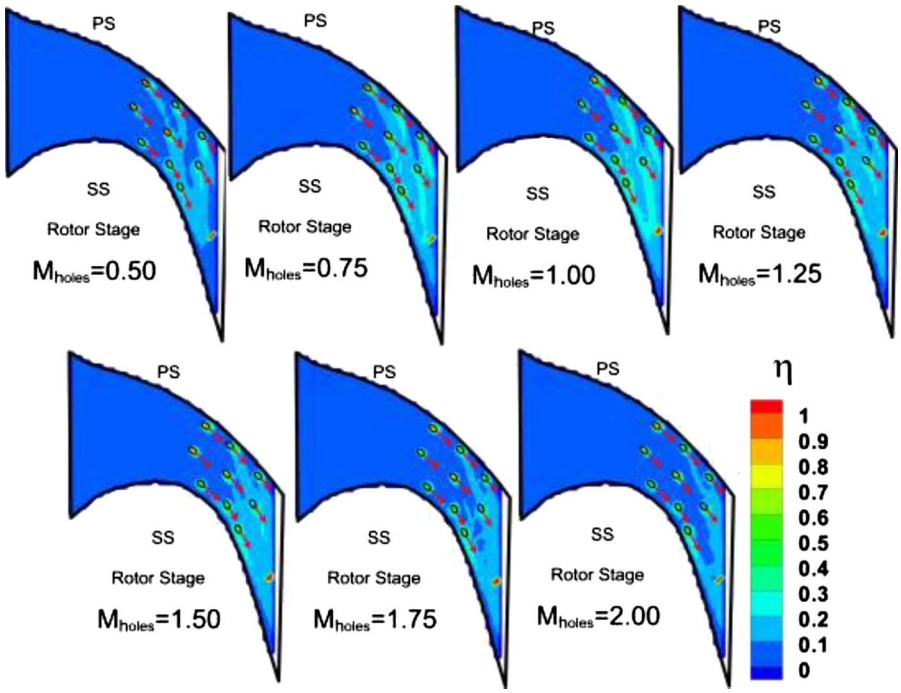

Fig. 11 Film-cooling effectiveness distribution on the film-cooling holes for all blowing ratios at 3000 rpm

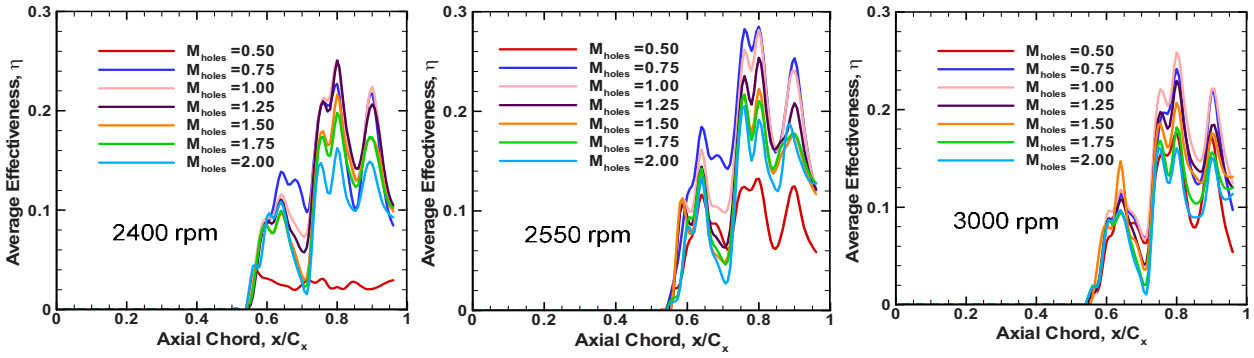

Fig. 12 Pitchwise average film-cooling effectiveness distribution along the axial chord for different turbine rotating speeds (M_{holes}=blowing ratio for holes)

mass necessary to maintain the same blowing ratio. This causes the $M_{holes}=1.00$ and 1.25 (higher coolant flow mass) to have a better effectiveness at 2400 rpm than the lower blowing ratios while at 2550 rpm and 3000 rpm, the best film protection is between $M_{holes}=0.75$ and 1.00, which has the ejected coolant mass comparable to $M_{holes}=1.00$ and 1.25 at 2400 rpm.

6.3 Pitchwise Average Film-Cooling Effectiveness. The film-cooling effectiveness data obtained for the three rotational speeds and all the blowing ratios are averaged pitchwise and plotted along the axial chord (Fig. 12) to study the effects of individual blowing ratios. The peaks on the plot represent the location of the holes on the platform in the axial direction. The holes are positioned to provide cooling to approximately 50% of the passageway. It is clearly seen that the effectiveness values are maximum for $M_{holes}=0.75-1.25$ for all three rotational speeds. For 2400 rpm, $M_{holes}=1.00$ and 1.25 have higher effectiveness as the coolant velocity and in turn the ejected coolant quantity are higher at these blowing ratios. Similarly, 2550 rpm and 3000 rpm have higher effectiveness magnitudes between $M_{holes}=0.75$ and 1.00. At these blowing ratios the coolant velocity and hence the coolant mass effectively suppress the effects of the secondary flow, leading to better coolant distribution on the platform surface. An increase in rotational speed causes the coolant exit velocity to increase for the same blowing ratio. To quantify the effects of rotation on film-cooling effectiveness, the pitchwise averaged film-cooling effectiveness was plotted along the axial chord for different rotational speeds but the same blowing ratio (Fig. 13). It is obvious from the plot that for the same blowing ratio, film-cooling effectiveness is maximum for the reference speed of 2550 rpm. The effectiveness magnitudes decrease on either side of the reference speed with 2400 rpm having slightly higher values as 3000 rpm as the flow conditions prevailing on the platform for 2400 rpm are much closer to the reference speed.

6.4 Combined Upstream Stator-Rotor Gap Purge Flow Cooling and Downstream Discrete-Hole Cooling. A combined platform cooling case involving coolant ejection through upstream

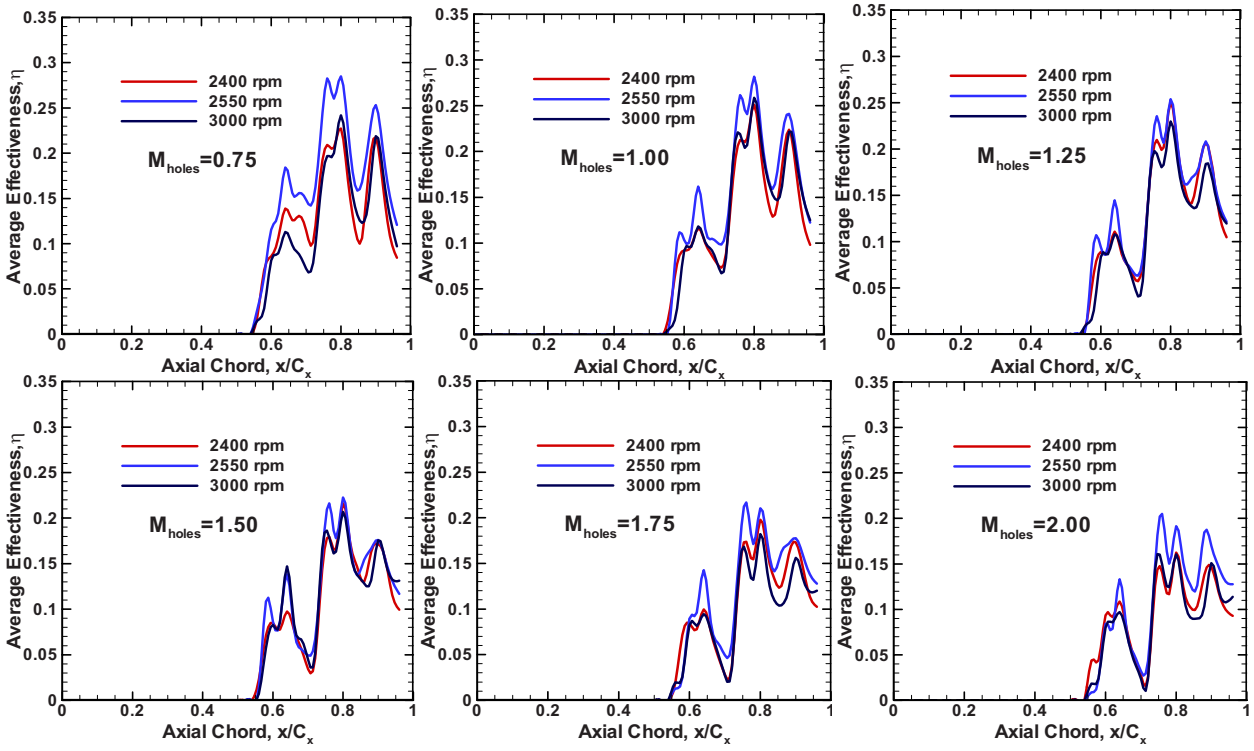

Fig. 13 Pitchwise average film-cooling effectiveness distribution along the axial chord for different hole blowing ratios (at different turbine rotating speeds)

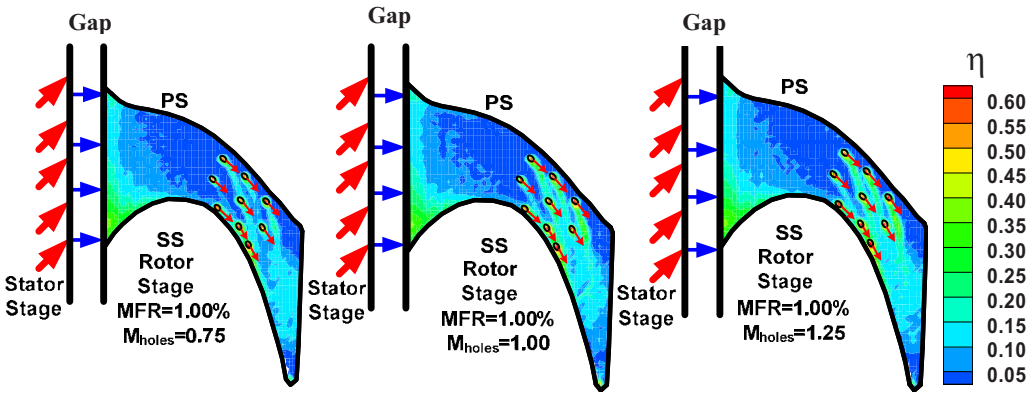

Fig. 14 Film-cooling effectiveness for combined stator-rotor gap and hole coolant injection, 2400 rpm

stator-rotor annular slot presented in a recent study by Suryanarayanan et al. [45] and downstream discrete holes was examined for 2400 rpm, 2550 rpm, and 3000 rpm to understand the interaction between the two methods of cooling under rotation. It is expected that the coolant ejected out of the slot will cover the platform front portion while the holes will provide protection in the downstream region. For the upstream blowing a coolant to mainstream mass flow ratio of 1% was considered as it was found to cover most of the upstream platform surface at all rotational speeds by Suryanarayanan et al. [45]. For the downstream hole blowing, $M_{\text{holes}}=0.75$, 1.00, and 1.25 were chosen as they provided the maximum film-cooling benefits. Film-cooling effectiveness data were acquired using PSP technique with coolant supplied simultaneously through both the loops. Temperatures of both the coolant loops were maintained the same as the mainstream flow to eliminate any temperature effects.

Figures 14–16 show the film-cooling effectiveness for the combined coolant ejection case for all three turbine rotational speeds. The inclined and horizontal arrows depict the mainstream and stator-rotor gap coolant flow, respectively. The figures also show the relative location of the stator-rotor upstream gap with respect to the blade leading edge. The coolant supplied through the stator-rotor gap as expected provides fairly good coverage in the upstream region though the distribution in the pitchwise direction is not uniform near the blade leading edge. Coolant concentration near the SS is greater than near the PS for all rotational speeds.

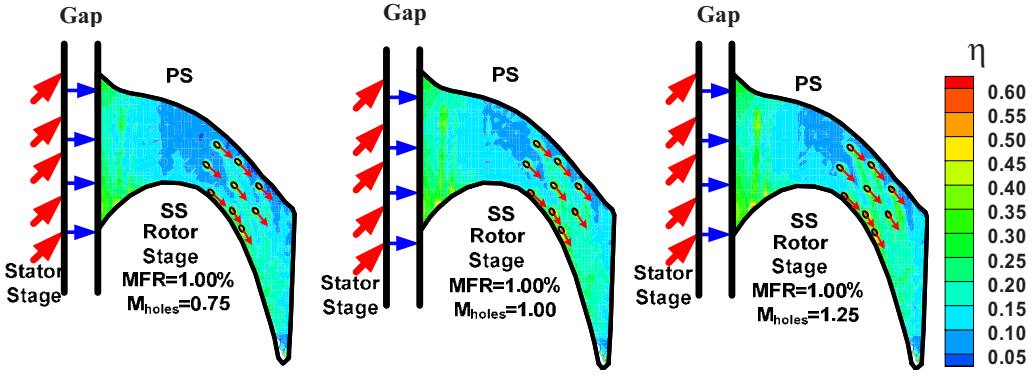

Fig. 15 Film-cooling effectiveness for combined stator-rotor gap and hole coolant injection, 2550 rpm

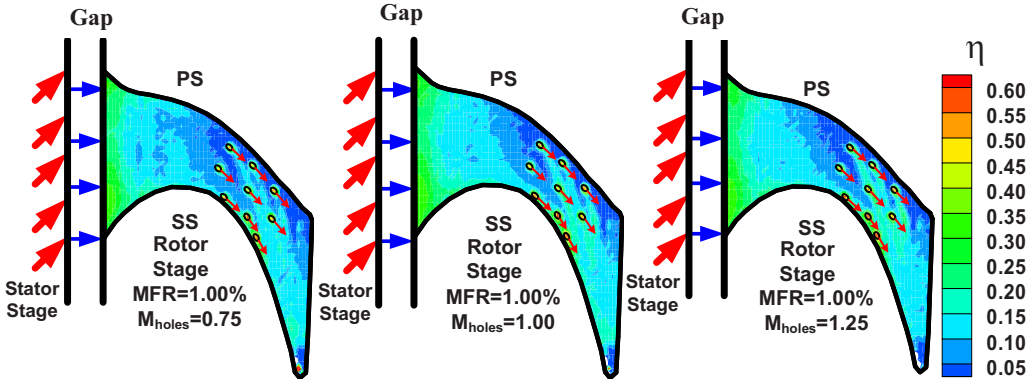

Fig. 16 Film-cooling effectiveness for combined stator-rotor gap and hole coolant injection, 3000 rpm

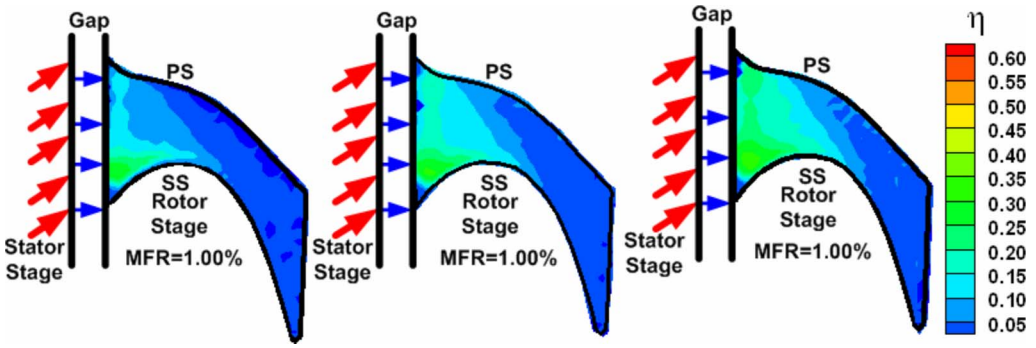

Fig. 17 Film-cooling effectiveness for stator-rotor gap injection for 2400 rpm, 2550 rpm, and 3000 rpm

The pressure gradient that persists between the pressure and suction surface of the blade tends to draw most of the coolant toward the suction side. At 2400 rpm, a strong vortex on the platform near the leading edge pressure side depletes any coolant supplied in this region and leads to lower effectiveness magnitudes. As the rotational speed is increased, the position of stagnation point on the leading edge changes. This movement of the stagnation point from the pressure surface leading edge for the lower rotational speed to the suction surface for the higher rotational speeds causes the pressure gradient $(\Delta P/\Delta S)$ across the platform between the suction side and the pressure side to decrease, leading to a much more uniform static pressure distribution on the platform surface. This reduction in the spanwise pressure gradient reduces the strength of the horse shoe vortex and allows for the spreading of the purge flow coolant on the platform surface, leading to higher effectiveness.

Also, the coolant exiting the gap, as it travels from the disk cavity into the rotating frame, undergoes a swirl due to the high shear associated with relative motion in the circumferential gap. This might cause some further spreading of the coolant on the platform surface for the higher rotor speeds. A little downstream of the leading edge near the pressure surface on the platform, the effect of upstream coolant ejection is drastically reduced as the passage vortex detaches from the pressure side and travels across the platform to merge with the suction side horse shoe vortex, diminishing the coolant coverage on the platform surface closer to the blade pressure side. These results are comparable to that seen in Fig. 17, which shows the film-cooling effectiveness distribution with just stator-rotor gap ejection for MFR=1.00% at all three rotational frequencies under consideration. The downstream hole blowing follows the trend seen in individual hole blowing cases discussed earlier. Reference rotation speed has the best spread and effectiveness magnitudes. Pitchwise averaged film-cooling effectiveness for the combined case is shown in Fig. 18. The results for the combined case reflect data for the individual blowing cases put together and give a comprehensive view of the appropriate upstream slot blowing MFR, average hole blowing ratio, and location of the coolant holes to provide appropriate coolant coverage for each rotational speed.

7 Conclusions

Film-cooling effectiveness measurements were performed on a rotating platform using PSP technique. Rotational speeds of 2400 rpm, 2550 rpm, and 3000 rpm were considered for the experiments to determine the effects of rotation on platform film cooling. Film-cooling effectiveness was quantified for downstream discrete-hole film cooling for M_{holes}=0.5, 0.75, 1.00, 1.25, 1.50, 1.75, and 2.00. Further, combined film-cooling tests were performed for an upstream stator-rotor gap purge flow ejection and downstream discrete-hole coolant ejection at MFR=1.00% and M_{holes}=0.75, 1.00, and 1.25. The results of the above research are summarized below.

1. Film-cooling effectiveness and coolant coverage on the rotor platform due to coolant ejection through downstream holes is maximum for the reference speed of 2550 rpm.
2. M_{holes} between 0.75 and 1.25 provided the best protection on the rotor platform for all three rotational speeds. Coolant coverage and effectiveness magnitudes were highest at these blowing ratios than the others tested. This result confirms that the blowing ratio of unity not only provides the best film coverage but it also minimizes the aerodynamic losses due to mixing of the cooling jets with the main flow.
3. Two downstream film-cooling holes (1 and 4 in Fig. 5) were

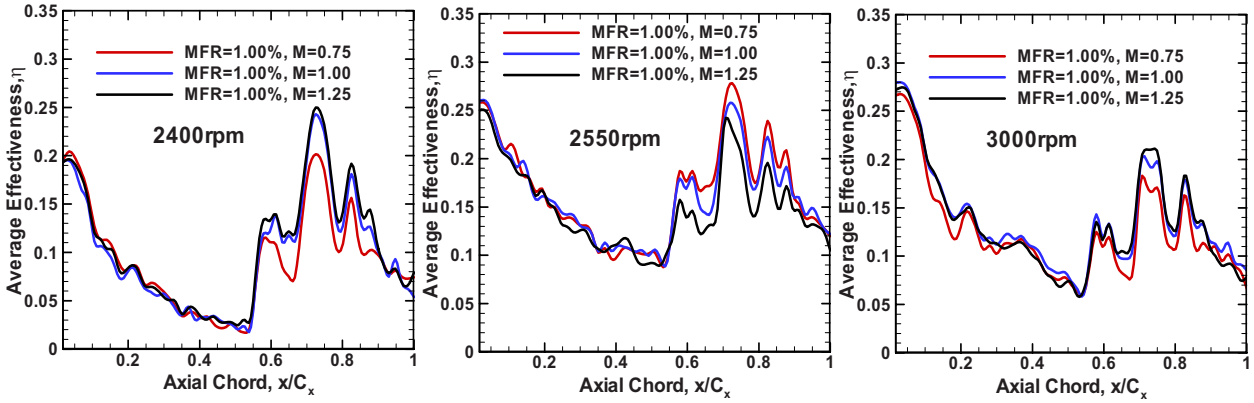

Fig. 18 Pitchwise averaged film-cooling effectiveness for combined upstream slot and downstream discrete-hole injection

affected more by the passage vortex than the other cooling holes, owing to their position on the rotor platform.
4. Secondary flow from the blade pressure surface to the suction surface strongly affected by the rotational motion caused the coolant traces from the holes to clearly flow toward the suction surface.
5. Complete film-cooling protection on a rotating platform can be provided with combined upstream stator-rotor gap ejection and discrete-hole ejection. Positioning the holes with angles oriented more toward the pressure surface will help reduce the effects of passage vortex and cross flow.
6. To optimize coolant usage, maintaining the stator-rotor gap injection close to MFR=1% and increasing the number of holes on the platform without compromising the structural integrity is the way forward in providing proper film protection on the platform.

Acknowledgment

This paper was prepared with the support of the U.S. Department of Energy, Office of Fossil Energy, National Energy Technology Laboratory. Hee-Koo Moon from Solar Turbines, Inc. provided the concept of the stator-rotor gap geometry in this study. C. Pang Lee from General Electric provided the concept of downstream discrete-hole geometry used in this study.

Nomenclature

C = oxygen concentration
C_x = axial chord length of the rotor blade (C_x =4.16 cm)
D = downstream coolant hole diameter (D=1 mm)
D_h = rotor diameter at the blade hub (cm)
D_t = rotor diameter at the blade tip (cm)
$f(P_{\text{ratio}})$ = relation between intensity ratio and pressure ratio
i = incidence flow angle change from design point at the first stage rotor inlet (deg)
I = pixel intensity for an image
M_{holes} = average blowing ratio ($M_{\text{holes}}=\rho_c V_c/\rho_m W_3$)
MFR = mass flow ratio (% of mainstream core flow)
LE = leading edge of the blade
M = Mach number
PS = pressure surface
P_{O_2} = partial pressure of oxygen
r = blade degree of the reaction
Ro = rotation number at first stage ($\text{Ro}=\Omega D_h/W_2$)
s = normal stator-rotor gap width (s=2.3 mm)
T_c = stator-rotor gap coolant temperature (°C)
V_c = average velocity of coolant from the holes (m/s)
U = tangential average velocity (m/s)
V = average absolute velocity of mainstream air (m/s)
V_u = tangential component of absolute velocity (m/s)
W = relative average velocity of mainstream air (m/s)
α = absolute velocity flow angle (deg)
β = relative velocity flow angle (deg)
γ = lateral coolant hole orientation angle (deg)
θ = streamwise coolant hole orientation angle (deg)
ΔP = static pressure difference on the platform across the pressure and suction surface of adjacent blades
ΔS = pitchwise incremental length on the platform across the pressure and suction surface of adjacent blades
ϕ = first stage flow coefficient, $\phi=V_{\text{ax}}/U_3$
λ = first stage load coefficient, $\lambda=(U_2V_{u_2}+U_3V_{u_3})/U_3^2$
η = local film-cooling effectiveness
ρ_c = density of coolant air (kg/m^3)
ρ_m = density of mainstream air at first stage rotor exit (kg/m^3)
Ω = turbine rotational frequency (rpm)

Subscript

1 = at first stage stator inlet
2 = at first stage stator exit (rotor inlet)
3 = at first stage rotor exit
x = axial distance from the blade leading edge (cm)
air = mainstream air along with air as a coolant
mix = mainstream air along with nitrogen as a coolant
ref = reference image with no mainstream and coolant flow
blk = image without illumination (black)

Superscript

* = lower rotating speeds than design point (2550 rpm)

References

[1] Schobeiri, M. T., 1999, "Efficiency, Performance and Flow Measurement of Siemens-Westinghouse HP-Turbine Blades," Series 9600 and 5600, Westinghouse Final Report.
[2] Schobeiri, M. T., Gilarranz, J. L., and Johansen, E. S., 2000, "Aerodynamic and Performance Studies of a Three Stage High Pressure Research Turbine With 3-D Blades, Design Points and Off-Design Experimental Investigations," ASME Paper No. 2000-GT-484.
[3] Schobeiri, M. T., Suryanarayanan, A., Jermann, C., and Neuenschwander, T., 2004, "A Comparative Aerodynamic and Performance Study of a Three-Stage High Pressure Turbine With 3-D Bowed Blades and Cylindrical Blades," ASME Paper No. GT-2004-53650.
[4] Lakshminarayana, B., 1996, *Fluid Dynamics and Heat Transfer of Turbomachinery*, Wiley, New York.
[5] Schobeiri, M., 2005, *Turbomachinery Flow Physics and Dynamic Performance*, Springer-Verlag, New York.
[6] Denton, J. D., 1993, "Loss Mechanisms in Turbomachines," ASME J. Turbomach., **115**, pp. 621–656.
[7] Langston, L. S., 1980, "Crossflow in a Turbine Cascade Passage," ASME J. Eng. Power, **102**, pp. 866–874.
[8] Goldstein, R. J., and Spores, R. A., 1988, "Turbulent Transport on the Endwall in the Region Between Adjacent Turbine Blades," ASME J. Heat Transfer, **110**, pp. 862–869.
[9] Takeishi, K., Matsuura, M., Aoki, S., and Sato, T., 1990, "An Experimental Study of Heat Transfer and Film Cooling on Low Aspect Ratio Turbine Nozzles," ASME J. Turbomach., **112**, pp. 488–496.
[10] Sieverding, C. H., 1985, "Recent Progress in the Understanding of Basic Aspects of Secondary Flows in Turbine Blade Passages," ASME J. Eng. Gas Turbines Power, **107**, pp. 248–257.
[11] Herzig, H. Z., Hansen, A. G., and Costello, G. R., 1953, "A Visualisation Study of Secondary Flows in Cascades," NACA Report No. 1163.
[12] Wang, H. P., Olson, S. J., Goldstein, R. J., and Eckert, E. G., 1995, "Flow Visualization in a Linear Turbine Cascade of High Performance Turbine Blades," ASME Paper No. 95-GT-7.
[13] Han, J. C., Dutta, S., and Ekkad, S. V., 2000, *Gas Turbine Heat Transfer and Cooling Technology*, Taylor & Francis, New York.
[14] Simon, T. W., and Piggush, J. D., 2006, "Turbine Endwall Aerodynamics and Heat Transfer," AIAA J., **22**(2), pp. 301–312.
[15] Bogard, D. G., and Thole, K. A., 2006, "Gas Turbine Film Cooling," AIAA J., **22**(2), pp. 249–270.
[16] Blair, M. F., 1974, "An Experimental Study of Heat Transfer and Film Cooling on Large-Scale Turbine Endwalls," ASME J. Heat Transfer, **96**, pp. 524–529.
[17] Harasgama, S. P., and Burton, C. D., 1992, "Film Cooling Research on the Endwall of a Turbine Nozzle Guide Vane in a Short Duration Annular Cascade: Part 1—Experimental Technique and Results," ASME J. Turbomach., **114**, pp. 734–740.
[18] Friedrichs, S., Hodson, H. P., and Dawes, W. N., 1996, "Distribution of Film-Cooling Effectiveness on a Turbine Endwall Measured Using Ammonia and Diazo Technique," ASME J. Turbomach., **118**, pp. 613–621.
[19] Friedrichs, S., Hodson, H. P., and Dawes, W. N., 1997, "Aerodynamic Aspects of Endwall Film-Cooling," ASME J. Turbomach., **119**, pp. 786–793.
[20] Chyu, M. K., 2001, "Heat Transfer Near Turbine Nozzle Endwall," Ann. N.Y. Acad. Sci., **934**, pp. 27–36.
[21] Zhang, L. J., and Jaiswal, R. S., 2001, "Turbine Nozzle Endwall Film Cooling Study Using Pressure Sensitive Paint," ASME J. Turbomach., **123**, pp. 730–

738.
[22] Kost, F., and Nicklas, M., 2001, "Film-Cooled Turbine Endwall in a Transonic Flow Field: Part 1—Aerodynamic Measurements," ASME J. Turbomach., **123**, pp. 709–719.
[23] Nicklas, M., 2001, "Film-Cooled Turbine Endwall in a Transonic Flow Field: Part 2—Heat Transfer and Film-Cooling Effectiveness," ASME J. Turbomach., **123**, pp. 720–728.
[24] Kost, F., and Mullaert, A., 2006, "Migration of Film-Coolant From Slot and Hole Ejection at a Turbine Vane Endwall," ASME Paper No. GT2006-90355.
[25] Oke, R. A., Simon, T. W., Burd, S. W., and Wahlberg, R., 2000, "Measurements in a Turbine Cascade Over a Contoured Endwall: Discrete Hole Injection of Bleed Flow," ASME Paper No. 2000-GT-214.
[26] Oke, R. A., Simon, T. W., Shih, T., Zhu, B., Ling, Y. L., and Chyu, M., 2001, "Measurements Over a Film-Cooled Contoured Endwall With Various Injection Rates," ASME Paper No. 2001-GT-140.
[27] Oke, R. A., and Simon, T. W., 2002, "Film Cooling Experiments With Flow Introduced Upstream of a First Stage Nozzle Guide Vane Through Slots of Various Geometries," ASME Paper No. GT-2002-30169.
[28] Knost, D. G., and Thole, K. A., 2004, "Adiabatic Effectiveness Measurements of Endwall Film-Cooling for a First Stage Vane," ASME Paper No. GT-2004-53326.
[29] Zhang, L., and Moon, H. K., 2003, "Turbine Nozzle Endwall Inlet Film Cooling—The Effect of a Back-Facing Step," ASME Paper No. GT-2003-38319.
[30] Piggush, J. D., and Simon, T. W., 2005, "Flow Measurements in a First Stage Nozzle Cascade Having Endwall Contouring, Leakage and Assembly Features," ASME Paper No. GT-2005-68340.
[31] Cardwell, N. D., Sundaram, N., and Thole, K. A., 2005, "Effects of Mid-Passage Gap, Endwall Misalignment and Roughness on Endwall Film-Cooling," ASME Paper No. GT-2005-68900.
[32] Hada, S., and Thole, K. A., "Computational Study of a Mid Passage Gap and Upstream Slot on Vane Endwall Film Cooling," ASME Paper No. GT-2006-91067.
[33] Barigozzi, G., Franchini, G., and Perdichizzi, A., 2006, "Endwall Film Cooling Through Fan-Shaped Holes With Different Area Ratios," ASME Paper No. GT-2006-90684.
[34] Dring, R. P., Blair, M. F., and Hoslyn, H. D., 1980, "An Experimental Investigation of Film Cooling on a Turbine Rotor Blade," ASME J. Eng. Power, **102**, pp. 81–87.
[35] Takeishi, M., Aoki, S., Sato, T., and Tsukagoshi, K., 1992, "Film Cooling on a Gas Turbine Rotor Blade," ASME J. Turbomach., **114**, pp. 828–834.
[36] Abhari, R. S., and Epstein, A. H., 1994, "An Experimental Study of Film Cooling in a Rotating Transonic Turbine," ASME J. Turbomach., **116**, pp. 63–70.
[37] Blair, M. F., 1994, "An Experimental Study of Heat Transfer in a Large-Scale Turbine Rotor Passage," ASME J. Turbomach., **116**, pp. 1–13.
[38] Ahn, J., Schobeiri, M. T., Han, J. C., and Moon, H. K., 2004, "Film Cooling Effectiveness on the Leading Edge of a Rotating Turbine Blade," ASME Paper No. IMECE 2004-59852.
[39] Ahn, J., Schobeiri, M. T., Han, J. C., and Moon, H. K., 2005, "Film Cooling Effectiveness on the Leading Edge of a Rotating Film-Cooled Blade Using Pressure Sensitive Paint," ASME Paper No. GT-2005-68344.
[40] Wright, L. M., Gao, Z., Varvel, T. A., and Han, J. C., 2005, "Assessment of Steady State PSP, TSP and IR Measurement Techniques for Flat Plate Film Cooling," ASME Paper No. HT-2005-72363.
[41] Gao, Z., Wright, L. M., and Han, J. C., 2005, "Assessment of Steady State PSP and Transient IR Measurement Techniques for Leading Edge Film Cooling," ASME Paper No. IMECE-2005-80146.
[42] Wright, L. M., Gao, Z., Yang, H., and Han, J. C., 2006, "Film Cooling Effectiveness Distribution on a Gas Turbine Blade Platform With Inclined Slot Leakage and Discrete Hole Flows," ASME Paper No. GT-2006-90375.
[43] Ahn, J., Mhetras, S. P., and Han, J. C., 2004, "Film-Cooling Effectiveness on a Gas Turbine Blade Tip," ASME Paper No. GT-2004-53249.
[44] Mhetras, S. M., Yang, H., Gao, Z., and Han, J. C., 2005, "Film Cooling Effectiveness on Squealer Rim Walls and Squealer Cavity Floor of a Gas Turbine Blade Tip Using Pressure Sensitive Paint," ASME Paper No. GT-2005-68387.
[45] Suryanarayanan, A., Mhetras, S., Schobeiri, M. T., and Han, J. C., "Film Cooling Effectiveness on a Rotating Turbine Platform Using Pressure Sensitive Paint Technique," ASME Paper No. GT-2006-90034.
[46] Schobeiri, M. T., 1989, "Optimum Trailing Edge Ejection for Cooled Gas Turbine Blades," ASME J. Turbomach., **111**(4), pp. 510–514.
[47] Schobeiri, M. T., and Pappu, K., 1999, "Optimization of Trailing Edge Ejection Mixing Losses Downstream of Cooled Turbine Blades: A Theoretical and Experimental Study," ASME J. Fluids Eng., **121**, pp. 118–125.
[48] McLachlan, B., and Bell, J., 1995, "Pressure-Sensitive Paint in Aerodynamic Testing," Exp. Therm. Fluid Sci., **10**, pp. 470–485.
[49] Coleman, H. W., and Steele, W. G., 1989, *Experimentation and Uncertainty Analysis for Engineers*, Wiley, New York.
[50] Holman, J. P., 2000, *Experimental Methods for Engineers*, McGraw-Hill, New York.